Selective uptake of La3+ ions with polyoxometalates-functionalized mesoporous SBA-15: An EXAFS study

Ourania Makrygenni, Faiza Lilia Bentaleb, Dalil Brouri, Anna Proust, Franck Launay, Richard Villanneau

Selective Uptake of La^{3+} ions with Polyoxometalates-functionalized Mesoporous SBA-15: an EXAFS Study.

Ourania Makrygenni,[a] *Faiza Lilia Bentaleb,*[a] *Dalil Brouri,*[b] *Anna Proust,*[a] *Franck Launay,*[b] *Richard Villanneau*[a]*

[a] Sorbonne Université, CNRS UMR 8232, Institut Parisien de Chimie Moléculaire, Campus Pierre et Marie Curie, 4 Place Jussieu, F-75005 Paris, France.

[b] Sorbonne Université, CNRS UMR 7197, Laboratoire de Réactivité de Surface, Campus Pierre et Marie Curie, 4 Place Jussieu, F-75005 Paris, France.

KEYWORDS: EXAFS; Polyoxometalates; Mesoporous silica; Lanthanum;

SYNOPSIS

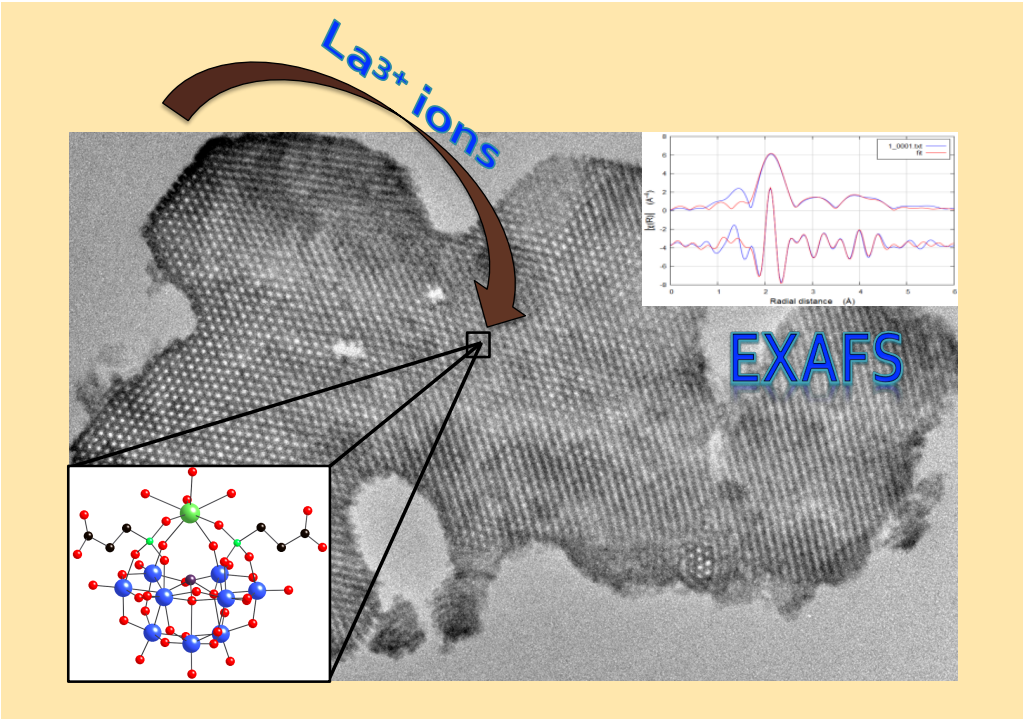

La^{3+} ions were incorporated into an organic/inorganic hybrid mesoporous SBA-15 functionalized with polyoxometalates (POMs). EXAFS spectroscopy at the La L_{III} edge gave definitive clues for a selective uptake of the incorporated La^{3+} ions by the POMs grafted onto the mesoporous supports, due to their chelate effect even in the presence of competitive adsorption sites.

ABSTRACT. In this work, mesoporous materials based on inorganic/organic polyoxometalate (POM) hybrids with the ability of further incorporating heterometallic lanthanum cations were designed. On the basis of the La^{3+} coordination to vacant organophosphonyle derivatives of POMs previously studied, herein POMs-grafted onto an amino-functionalized mesoporous SBA-15 ({NH_2}-SBA-15) with incorporated La^{3+} ions were synthesized with various amounts of La^{3+}. L_{III}-edge La EXAFS spectroscopy of the resulting materials provided local structural information

around La^{III} ions (*i.e.* number, nature and distances of neighboring atoms), which are comparable to that of the La^{III} complexes of POMs hybrids. This technique, in addition with ^{31}P CP-MAS NMR spectroscopy, gave definitive clues for a selective uptake of the incorporated La^{3+} ions by the POMs grafted onto the $\{NH_2\}$-SBA-15 supports. This study is a clear demonstration that, due to their chelate effect, POMs hybrids act as efficient ligands for La^{3+} even in the presence of competitive adsorption sites. Consequently, a regular distribution of the La^{3+} ions along the channels of the SBA-15 is thus observed in these materials due to the nanostructuration of the POMs onto the support.

Introduction

One property of polyoxometalates (POMs), among others, is that they are transition metal oxoanion nanosized clusters stable against hydrolysis (assuming that the pH is controlled) and toward strong oxidation conditions.[1] POMs, including their transition metal derivatives, have been thus thoroughly considered as intrinsic oxidation catalysts either in homogeneous or heterogeneous conditions.[2] Furthermore, lacunary (or vacant) complexes may be obtained through basic degradation of complete species by formal removal of one or several oxo metal fragments. The chemistry of such lacunary species has been widely studied during the 60s to 90s, in particular in the case of Keggin or Dawson type heteropolyanions.[3] These vacant species are capable to act as versatile multidentate inorganic ligands with strong chelate effects, due to the presence of nucleophilic oxygen atoms that delimitate the lacuna. Since they are π-donor (*via* the oxo ligands) and π-acceptor ligands (*via* the d^0 metal centers) simultaneously, they are able to accommodate cations in a wide range of oxidation states.[4] In parallel, these lacunary species may be also functionalized by organic groups, since they are able to react with one or several organic derivatives from the p block (organosilanes, organophosphonates, organoarsonates,

organostannates, alkoxides).[5] This led to a class of compounds that were defined as organic/inorganic hybrid derivatives of POMs. Among these, the bis-organophosphonyle/arsonyle derivatives of trivacant Keggin-type POMs were more recently reconsidered as a new class of catalysts that offer some great advantages in comparison with classical POMs and transition metal substituted POMs. Firstly, they are able to covalently bind to an inorganic support using different linking strategies due to the presence of useful organic functions.[6],[7],[8] Furthermore this covalent immobilization strategy came along with an excellent dispersion on various silica supports, all along the channels of mesoporous SBA-15 materials[9] or at the silica surface of magnetic core-shell nanoparticles.[7] These two properties should be seen as criteria that meet the expectations of an efficient heterogenized catalyst, especially since the existence of a covalent link does not prevent the catalytic reactivity of these supported systems.[9]

In addition, it has also been shown that some POMs hybrids may still play the role of multidentate ligands towards metal cations from different families of the periodic table (lanthanides, alkaline earth metals and transition metals).[10] Indeed, due to the presence of {P=O} or {As=O} coordinating functions, vacant organophosphonyle/arsonyle derivatives of POMs can be considered as hard ligands (regarding the HSAB classification), since “soft” cations are hardly bound to their coordination sites.[11] In this regard, POMs hybrids based on the anions A-α-$[PW_9O_{34}\{P/As(O)R\}_2]^{5-}$ and B-α-$[AsW_9O_{33}\{P/As(O)R\}_2]^{5-}$ (with R = ^{t}-Bu, C_6H_5, *p*-C_6H_4-NH_2 and $CH_2CH_2CO_2H$) were able to form with La^{3+} and Ce^{3+} cations discrete 1:1 complexes in which the cations are bound to the oxygen atoms of the $\{XW_9\}$ units and/or the {RP/As=O} groups.

Thus, the reaction carried out for the synthesis of these hybrids with La consists in mixing the functionalized POMs with different equivalents of $La(NO_3)_3.6H_2O$ at room temperature in polar organic solvents such as acetonitrile. Complexes of lanthanum ions with a 1:1 POM/La^{3+} stoichiometry were systematically obtained. After recrystallization in *N,N*-dimethyl-formamide, the structure of the resulting complexes was obtained by single crystal X-ray diffraction analysis. **Figure 1** shows the details of the structures of two examples of these metallic derivatives of POMs hybrids, namely $[PW_9O_{34}\{As(O)C_6H_4\text{-}p\text{-}NH_2\}_2\{La(dmf)_5(H_2O)\}]^{2-}$ and $[AsW_9O_{33}\{P(O)CH_2CH_2CO_2H\}_2\{La(dmf)(H_2O)_2\}]^{2-}$.

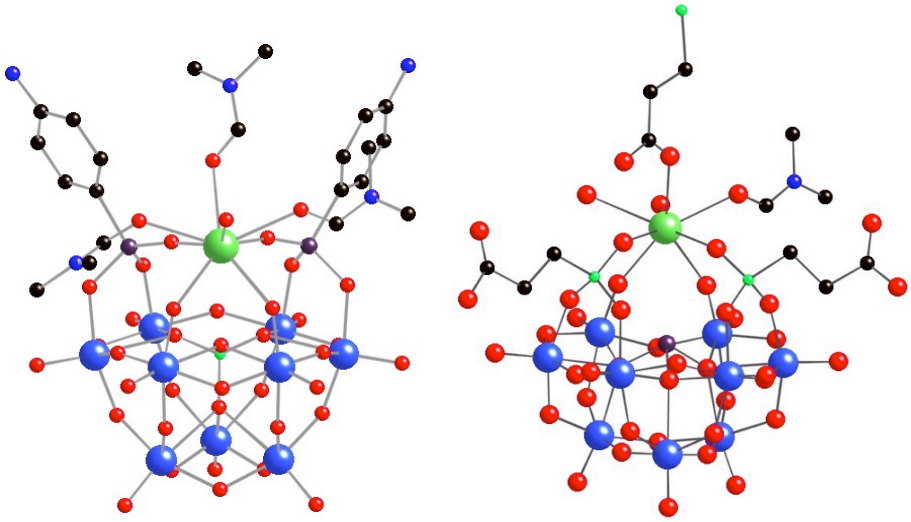

Figure 1. Structure of anion $[PW_9O_{34}\{As(O)C_6H_4\text{-}p\text{-}NH_2\}_2\{La(dmf)_3(H_2O)_2\}]^{2-}$ (La⊂POM-NH_2, left) and details of the coordination of La^{3+} ions in $[AsW_9O_{33}\{P(O)CH_2CH_2CO_2H\}_2\{La(dmf)(H_2O)_2\}]^{2-}$ (La⊂POM-COOH, right). *P, C, O, As and N atoms are respectively represented as small green, black, red, prune and blue balls. W and La cations are respectively represented as large blue and green balls.*

This affinity for the largest lanthanides cations is particularly interesting since these cations (especially La^{3+}) are regularly used as harmless and highly efficient Lewis acid catalysts

in various reactions in fine chemistry such as transesterification,[12] Diels-Alder[13] and Friedel-Craft[14] in homogeneous conditions. The immobilization of lanthanide cations on an inert support and their use as single-site heterogeneous catalysts remains however a challenge.[15] This is obviously due to the lability of lanthanides (+III) ions that generally prevents strong linkage to a support, even if it is possible to directly incorporate La^{III} ions in the framework of a SBA-15 silica by a direct synthesis strategy.[16] In the present work, we addressed the design of hybrid systems based on the incorporation of La^{3+} cations into POMs-supported amino-functionalized SBA-15. In this study, we used EXAFS spectroscopy at the La L_{III}-edge in order to specifically localize the La^{3+} cations in the materials and to determine whether the immobilized POMs hybrids retained their chelating properties.

Experimental Section

Solvents and other reagents were obtained from commercial sources and used as received. The complexes $(^{n}Bu_4N)_3NaH[As^{III}W_9O_{33}\{P(O)(CH_2CH_2CO_2H)\}_2]$ - (POM-COOH) - and $(^{n}Bu_4N)_4H[PW_9O_{34}\{As(O)(C_6H_4NH_2)\}_2]$ - ($POM\text{-}NH_2$) – and their lanthanum complexes were prepared as previously described.[10],[11] The syntheses of POM-COOH and of $[AsW_9O_{33}\{P(O)CH_2CH_2CO_2H\}_2\{La(dmf)(H_2O)_2\}]^{2-}$ (La⊂POM-COOH) were added in Supporting Information. The amino-functionalized SBA-15 (for short $\{NH_2\}$-SBA-15) was obtained in a two-steps procedure, by the functionalization of a pre-formed SBA-15 with 3-aminopropyltriethoxysilane (initial loading of $-NH_2$ groups: 2.12 mmol g^{-1}).[6] The grafting of POM-COOH onto $\{NH_2\}$-SBA-15 was performed according to the procedure previously described (0.1 mmol.g^{-1} of POM-COOH in POM-COOH@$\{NH_2\}$-SBA-15 materials).[6]

The $\{^1H\}$ ^{31}P NMR (121.5 MHz) solution spectra were recorded in 5 mm o.d. tubes on a Bruker Avance 300 spectrometer equipped with a QNP probehead. The ^{31}P MAS NMR spectra were

recorded at 283.31 MHz on a Bruker AVANCE III 700 spectrometer (16.4 T) equipped with 2.5 mm Bruker probe and at a spinning frequency of 30 kHz. Chemical shifts were referenced to 85% aqueous H_3PO_4 for ^{31}P. X-Ray Fluorescence analyses were conducted with an energy dispersive spectrometer (XEPOS with Turboquant powder software). HR-TEM analyses were realized on a microscope operating at 200 kV with a resolution of 0.18 nm (JEOL JEM 2011 UHR) equipped with an EDX system (PGT IMIX-PC). Samples were dispersed in resin and cut with an ultramicrotome. The lamellas of 50 nm thickness were then deposited on Cu grids covered with an amorphous carbon film.

The preparation of the different mesoporous silica supports (*i.e.* {NH_2}-SBA-15 and POM-COOH@{NH_2}-SBA-15) that incorporate La^{3+} with various amounts (La@{NH_2}-SBA-15 and La⊂POM-COOH@{NH_2}-SBA-15(x:1) respectively) are described in the supplementary information.

Results and discussion

In this study, we thus focused on studying the complexation of La^{3+} of hybrid derivatives of POMs in the solid state, after their immobilization onto a mesoporous oxide support. This study was thus performed by combining ^{31}P MAS NMR, XAS and X-EDS spectroscopies. Prior to the presentation of the results, it seems to be relevant to remind of some elements of characterization that concerned the complexes obtained with La^{3+} and the organophosphonyle/arsonyle derivatives of POMs.

1. Characterization of the molecular model compound $[AsW_9O_{33}\{P(O)CH_2CH_2CO_2H\}_2\{La(dmf)(H_2O)_2\}]^{2-}$

As mentioned in the introduction, A-α-$[PW_9O_{34}\{As(O)\text{-}p\text{-}C_6H_4\text{-}NH_2\}_2]^{5-}$ (POM-NH_2) and B-α-$[AsW_9O_{33}\{P(O)CH_2CH_2CO_2H\ \}_2]^{5-}$ (POM-COOH) were able to form discrete 1:1 complexes

with La^{3+} cations, leading respectively to the formation of $[PW_9O_{34}\{As(O)C_6H_4\text{-}p\text{-}NH_2\}_2\{La(dmf)_3(H_2O)_2\}]^{2-}$ (La⊂POM-NH_2) and $[AsW_9O_{33}\{P(O)CH_2CH_2CO_2H\}_2\{La(dmf)(H_2O)_2\}]^{2-}$ (La⊂POM-COOH).[10],[11] As seen from the complete crystal structures (see figure S1), the anion $[AsW_9O_{33}\{P(O)CH_2CH_2CO_2H\}_2\{La(dmf)(H_2O)_2\}]^{2-}$ could be isolated in the solid state in a polymeric assembly. However, in both structures (La⊂POM-NH_2 and La⊂POM-COOH), the coordination polyhedron was constituted with 8 oxygen atoms. The details of the La-O distances in both complexes are displayed in supplementary Information (Table S1).

La⊂POM-COOH was characterized by multinuclear NMR spectroscopy, in particular by ^{31}P NMR (see Table 1). The comparison of the spectroscopic data of the two complexes (without and with La^{3+}) is instructive since the chemical shifts associated to the {P=O} groups in both complexes are significantly different. This is in accordance with the fact that the complexation of La^{3+} involves the {P=O} groups in $[AsW_9O_{33}\{P(O)CH_2CH_2CO_2H\}_2\{La(dmf)(H_2O)_2\}]^{2-}$.

	$^{31}P\{^1H\}$
	***δ* (ppm)**
La⊂POM-COOH	19.1
POM-COOH	29.0

Table 1. Chemical shift of $^{31}P\{^1H\}$ spectra (in a 2:1 mixture of dmf/CD_3CN) for the anions $[AsW_9O_{33}\{P(O)CH_2CH_2CO_2H\}_2\{La(dmf)(H_2O)_2\}]^{2-}$ (La⊂POM-COOH) and $[AsW_9O_{33}\{P(O)CH_2CH_2CO_2H\}_2]^{5-}$ (POM-COOH).

Thus, the results presented in this paragraph are of great interest for the characterization of the supported La^{3+} complexes, as the molecular complexes mentioned above will be used as models for the XAS characterization.

2. Preparation and characterization of supported polyoxometalate hybrids containing La^{3+} ions: La⊂POM-COOH@{NH_2}-SBA-15

The preparation of the supported polyoxometalate hybrids, here POM-COOH@{NH_2}-SBA-15,was performed according to our classical covalent grafting strategy, i.e. by formation of an amide link by the reaction of the carboxylic groups of the POM-COOH and the {NH_2} functions of the {NH_2}-SBA-15.[6] Subsequently, La^{3+} ions were incorporated into POM-COOH@{NH_2}-SBA-15. A first preliminary sample was prepared by dispersion of POM-COOH@{NH_2}-SBA-15 with an excess of $La(NO_3)_3{\cdot}6H_2O$ (3 equiv. of La^{3+} per POM-COOH) dissolved in 10 mL of acetonitrile (see SI for the details of the synthesis). The supernatant was then removed by filtration. The sample was analyzed by X-EDS, and the final W/La ratio was found equal to 2.67 (average value obtained from 10 independent measurements), which roughly corresponds to the expected La/POM-COOH ratio introduced (theoretical: 3:1, experimental 3.3:1).

This preliminary sample La⊂POM-COOH@{NH_2}-SBA-15 was characterized by High Resolution Transmission Electronic Microscopy (HR-TEM), and two micrographs of this sample (after microtome cuttings) at different magnifications are displayed on figure 2. At low magnification (left), the micrographs confirmed that the long-range structure of the SBA-15 was maintained after the different grafting steps (*i.e.* functionalization with APTES, covalent grafting of the POMs and incorporation of the La(III) cations). Furthermore, at higher magnification it was also possible to observe the regular distribution of the grafted POMs around the pores, as stated in our previous works (see also figure S2 for additional micrographs of the preliminary sample La⊂POM-COOH@{NH_2}-SBA-15 showing the distribution of the POMs all along the channels of the SBA-15, at different orientations).

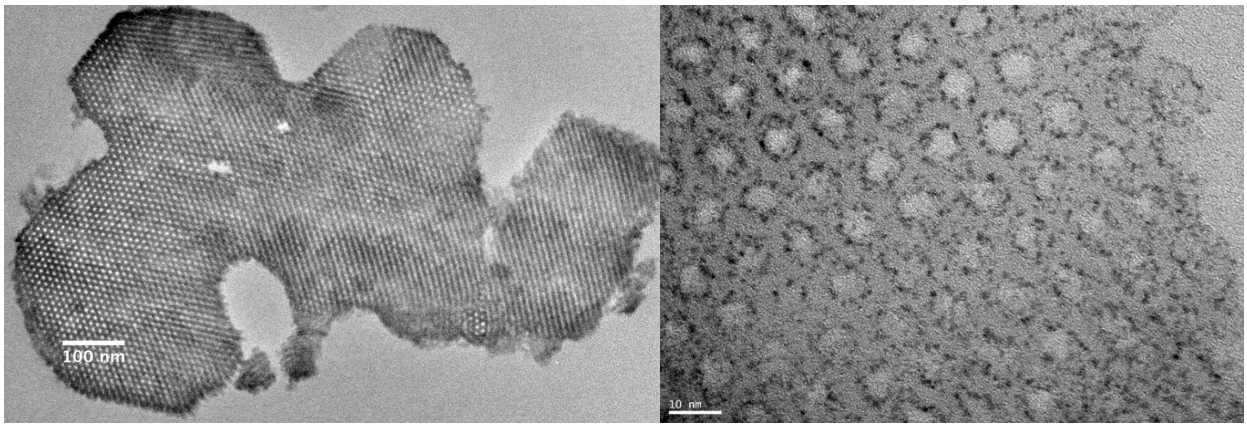

Figure 2. HR-TEM micrographs (after microtome cuttings) of La⊂POM-COOH@{NH_2}-SBA-15 at different magnifications showing the retention of the structure of the SBA-15 after the different grafting steps.

In addition, the ^{31}P CP-MAS NMR spectrum of the preliminary La⊂POM-COOH@{NH_2}-SBA-15 solid sample was recorded and compared to that of the initial solid sample of POM-COOH@{NH_2}-SBA-15 (Figure 3). The chemical shift of the samples decreased from 27.9 ppm for POM-COOH@{NH_2}-SBA-15 to 22.2 ppm for the sample incorporating La^{3+}. This significant shift followed the trend observed in acetonitrile for the homogeneous system (table 1) and indicates that the coordination of La^{3+} ions with POM-COOH also occurred in the solid state in the presence of an excess of lanthanum.[a]

[a] The difference between the experimental ^{31}P NMR chemical shifts of the free POM-COOH and their La^{3+} complex in solution is larger than the solid state. In a general way, the numeric value of a chemical shift strongly depends on the environment of the chemical species studied. The chemical shifts in Table 1, obtained with a 2:1 dimethylformamide:CD_3CN mixture, are both slightly different from the absolute values of the chemical shifts before and after complexation in the solid state. It is however rather difficult to rationalize these differences without the help of computational chemistry. Furthermore, the hypothesis of the existence of POMs in the materials that did not coordinate La^{3+} ions cannot be ruled out (even with an excess of La^{3+}) if part of the POMs are not accessible for instance. In this case, the ^{31}P NMR chemical shift experimentally observed would be an average value between POMs that coordinates La^{3+} or not.

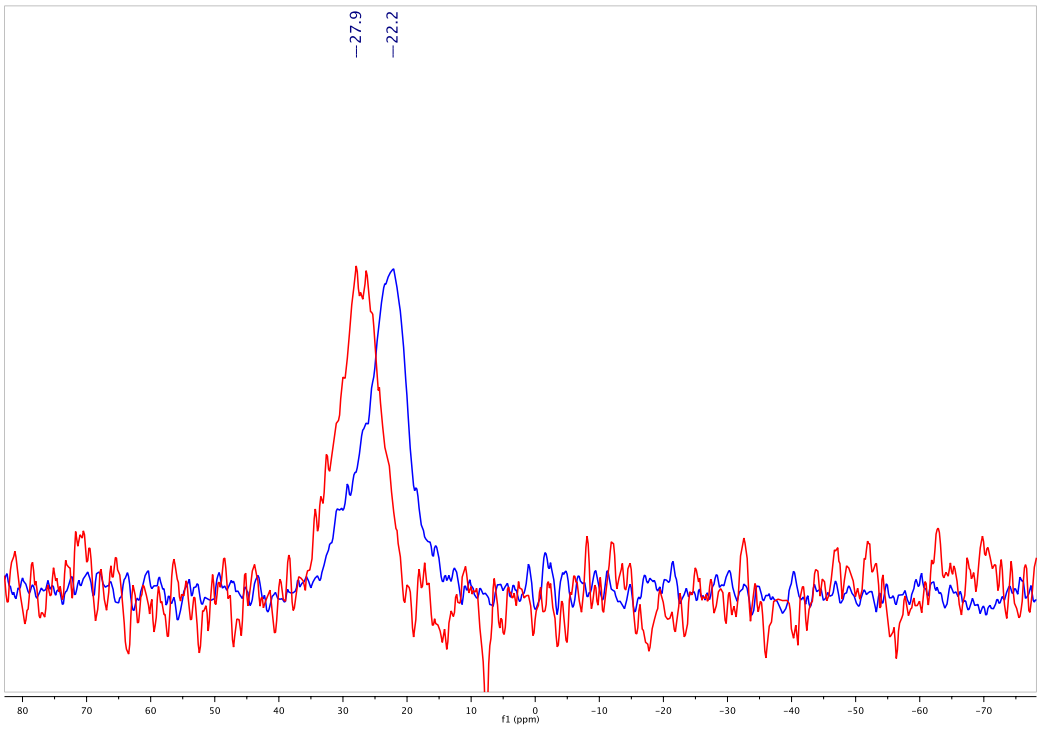

Figure 3. ^{31}P CP-MAS NMR spectra of La⊂POM-COOH@{NH_2}-SBA-15 (in blue) and of POM-COOH@{NH_2}-SBA-15 (in red).

In order to obtain a definitive clue for a selective La^{3+} uptake by the POMs in the final materials, a XAS study at the La L_{III} edge was performed. Three additional materials were prepared by wet impregnation of POM-COOH@{NH_2}-SBA-15 with various amounts of $La(NO_3)_3{\cdot}6H_2O$. The later was calculated in order to have a final ratio La/POMs-COOH x = 0.75, 1, and 2. The three samples denoted La⊂POM-COOH@{NH_2}-SBA-15(x:1) were also characterized by TEM and X-EDS. Table 2 gives the La/POM ratio in each compound (average value on 6 independent measurements for each sample).

La/POM theor. Ratio (x)	0.75	1	2
La/POM exp. ratio	0.85	0.93	1.93

Table 2: Theoretical and experimental (determined by X-EDS) La/POM ratio for La⊂POM-COOH@{NH_2}-SBA-15(x:1) with x = 0.75, 1 and 2.

The pore properties of the different materials were analyzed from their nitrogen adsorption-desorption isotherms and their Brunauer-Emmet-Teller (BET) surface areas; the results are shown in Figure S3 and Table 3. The N_2 adsorption-desorption isotherms of the SBA-15 based materials exhibited characteristic type IV patterns, which indicated that all materials were constituted of mesoporous channels with rather uniform diameters. The textural parameters (S_{BET} value, mean pore diameter and pore volume) obtained with POM-COOH@{NH_2}-SBA-15 and all three La⊂POM-COOH@{NH_2}-SBA-15(x:1) were in the same order of magnitude indicating that the introduction of the La^{3+} cations did not modify significantly the porosity of the materials, in accordance with a specific uptake of the ions by the grafted POMs. It is however noteworthy that the textural parameters of the La⊂POM-COOH@{NH_2}-SBA-15(2:1) were particularly low probably for the higher amount of $La(NO_3)_3 \cdot 6H_2O$ introduced.

	S_{BET} ($m^2.g^{-1}$)	Pore Vol. ($cm^3.g^{-1}$) (desorption)	Pore diam. (nm) (desorption)
{NH_2}-SBA-15	595	0.69	5.8
POM-COOH@{NH_2}-SBA-15	185	0.33	4.7
La⊂POM-COOH@{NH_2}-SBA-15(0.75:1)	160	0.33	4.6
La⊂POM-COOH@{NH_2}-SBA-15(1:1)	164	0.25	4.65
La⊂POM-COOH@{NH_2}-SBA-15(2:1)	50	0.10	3.81

Table 3: textural parameters of {NH_2}-SBA-15, POM-COOH@{NH_2}-SBA-15 and of the different La⊂POM-COOH@{NH_2}-SBA-15(x:1).

All three materials La⊂POM-COOH@{NH2}-SBA-15(x:1) were characterized by small angle X-Ray Diffraction (Figure S4) and the corresponding diffractograms all displayed the characteristic patterns attributed to the hexagonal network of the SBA-15 based materials.

A control sample, denoted La⊂{NH_2}-SBA-15(1:1) was also prepared by wet impregnation of SBA-NH_2 with a solution of $La(NO_3)_3 \cdot 6H_2O$. The amount of $La(NO_3)_3 \cdot 6H_2O$ added here was the same as in La⊂POM-COOH@{NH_2}-SBA-15(1:1). Furthermore, the mass of POM-COOH@{NH_2}-SBA-15 and {NH_2}-SBA-15 supports used were chosen so that the number of -NH_2 functions was identical in both samples.

3. Extended X-ray Absorption Fine Spectroscopy Study of the materials.

A XAS study at the L_{III} edge of La at low temperature (70 K) was performed at Synchrotron SOLEIL in Saclay (SAMBA beamline) in order to better characterize the synthesized materials and especially to show the specific coordination of La^{3+} by the lacunary POM. EXAFS spectroscopy, in particular, is a powerful tool for the characterization of non-crystallized materials, being in solution, gas, or in the solid state. Indeed, it provides local structural information around a specific element (in the present study La^{III} ions), *i.e.* number and nature of neighboring atoms, but it can also provide the distances to these neighboring atoms. This spectroscopic technique has been parsimoniously utilized in the polyoxometalate community,[17] but examples do exist, especially in the field of catalysis.[18] In the present study, we used EXAFS technique in order to determine the exact location of the La^{3+} ions after their introduction onto the POM-COOH@{NH_2}-SBA-15 materials.

In addition, XANES spectra of samples may be recorded in parallel, providing information on the oxidation state of the targeted elements. However in this study, XANES was not useful since there is no ambiguity on the oxidation state of La.

3.1 EXAFS characterization of model compounds

EXAFS spectra at the La L_{III} edge were first recorded at solid state from the molecular models ($(^{n}Bu_4N)_2[PW_9O_{34}\{As(O)C_6H_4\text{-}p\text{-}NH_2\}_2\{La(dmf)_3(H_2O)_2\}]^{2-}$ (La⊂POM-NH_2) and $(^{n}Bu_4N)_2[AsW_9O_{33}\{P(O)CH_2CH_2CO_2H\}_2\{La(dmf)(H_2O)_2\}]^{2-}$ (La⊂POM-COOH) described before. Spectra analysis was conducted with the IFEFFIT library using the GUI Athena and Artemis.[19] For illustration purposes, the normalized absorption spectrum of a solid sample of La⊂POM-COOH is presented in Figure S5. The spectrum displayed two distinct absorption edges, corresponding respectively to the L_{III} (5490 eV) and L_{II} (5896 eV) edges. Due to the close proximity of the L_{II} edge, the absorption spectrum was cut at 5883 eV for all spectra. The E^0 value was fixed at 5489.5 eV and the normalization was done using a spline with *k* weight = 3 in the range of 5588-5883 eV for all spectra. The forward Fourier Transforms (FT) were obtained using a Kaiser-Bessel window (δk = 2) in the k space in the range of 3.6-8.8 $Å^{-1}$. The EXAFS signal (extracted from the absorption spectrum) and the corresponding FT of both compounds are displayed in Figure 4.

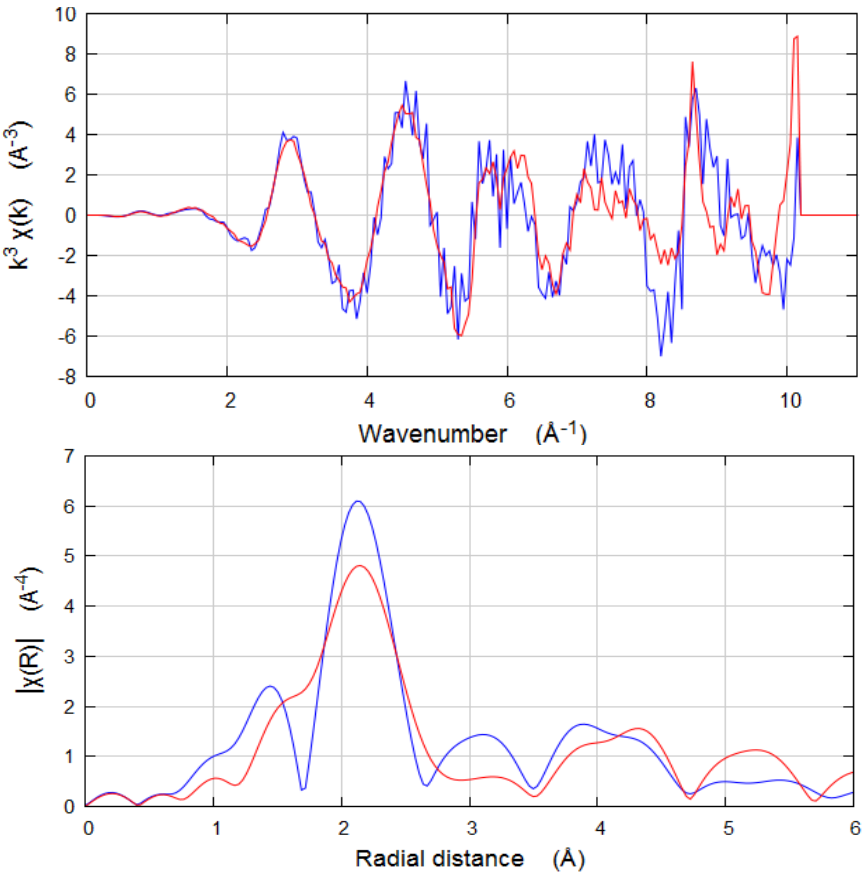

Figure 4. EXAFS signals (up) and FT (down) for compounds La⊂POM-COOH (in blue) and La⊂POM-NH_2 (in red).

Even if there are some differences in the structure of both complexes (distances and nature of atoms in the second shell of neighbors), the EXAFS spectra are relatively close, especially the mean values and the distribution of La-O distances. Consequently, the spectra of all samples used in this study will be compared to the spectrum of the complex La⊂POM-COOH as a unique model compound.

The EXAFS signal of La⊂POM-COOH was then modeled by using FEFF calculations[20] and the structural parameters (phases and amplitudes) were extracted from the X-ray data of the compound La⊂POM-COOH. Figure 5 shows the modulus and the real part of the FT for the experimental and calculated spectra of La⊂POM-COOH. The calculated structural parameters of

La⊂POM-COOH are gathered in Table 4. These results were obtained by taking into account the 8 different FEFF paths with the higher rank, from 89 calculated paths. These 8 paths then defined 3 individual neighboring shells, the 2nd and 3rd shell including several multiple scattering paths.

A single value of ΔE° (adjustment to the E° used in the normalization step) was fitted for all paths, while ΔR (adjustment of the interatomic distance) and $|\sigma^2|$ (mean square variation in path length) were respectively determined for all paths or shells.

These parameters are in close agreement with the X-ray structure obtained for this compound. For the purpose of comparison, the value for the average La-O distance obtained was 2.554 Å from X-ray data (see SI), compared to 2.622 Å in the present study. Even at long distance the FEFF calculations appear satisfying, since the experimental La-W distance is of 4.215 Å (X-ray data) while the FEFF calculation of the spectrum gave 4.178 Å. However, due to a relatively low signal over noise ratio at high R values, one might wonder about the relevance of the use of the third shell for the characterization of the following samples.

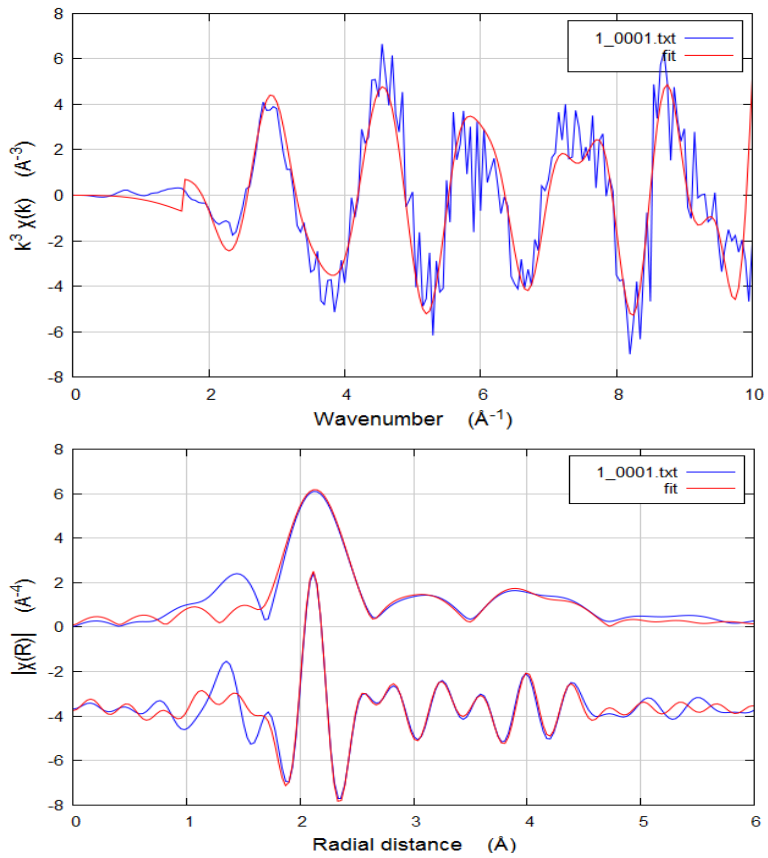

Figure 5. EXAFS spectrum (up), modulus and real part of the FT (bottom) for the experimental (in blue) and calculated (in red) spectra of La⊂POM-COOH.

Shell	Path	Nb of neighbors ($N.S_0^2$)	ΔE° (eV)	R (Å)	$\|\sigma^2\|$
1st shell	La-O	8	9.907 ± 0.830	2.622 ± 0.033	0.0061
2nd shell	La-As	1		3.618 ± 0.039	0.0058
	La-O-P *	2		3.969 ± 0.4.16	
	La-P	2		4.027 ± 0.376	
	La-C	2		3.970 ± 0.447	
	La-O-C *	2		3.350 ± 0.130	
3rd shell	La-W	2		4.178 ± 0.096	0.0086
	La-O-W *	4		3.893 ± 0.101	0.0009

Table 4. Calculated FEFF structural parameters of La⊂POM-COOH; * paths with multiple scattering.

3.2 EXAFS characterization of the La⊂POM-COOH@{NH_2}-SBA-15(x:1) materials

Figure 6 (top) displays the calculated and experimental FTs of the EXAFS spectrum for the first shell of the La⊂{NH_2}-SBA-15. In this sample, it was expected that the coordination sphere of the La^{3+} ions was constituted by a mixture of {-NH_2} originating from the propylamine functions grafted on the support, of remaining solvent molecules (predominantly water that can be found in the chemical reagent $La(NO_3)_3{\cdot}6H_2O$) and probably of oxygen atoms from residual silanol groups of the SBA-15. Assuming that it is rather difficult to precisely determine the ratio O/N by EXAFS in the coordination sphere of the lanthanum, the coordination sphere of the lanthanum in La⊂{NH_2}-SBA-15 was modeled using only O atoms. The structural data extracted from the FT were significantly different from those obtained for La⊂POM-COOH, for the first and second shells. Indeed, unlike the model compound, the La-O/N shell in La⊂{NH_2}-SBA-15 had to be calculated by using two sets of distances (3 oxygen atoms at 2.487 Å and 4 oxygen atoms at 2.668 Å). Furthermore, there is no peak in the FT corresponding to a second shell in the range 2.7 and 3.5 Å, which is consistent with the absence of As and P atoms from the POM-COOH in the environment of the La^{III} ions in La⊂{NH_2}-SBA-15. However, the presence of peaks in the range 3.5-4.5 Å is necessarily explained by the presence of noise since there is no heavy atom expected at this distance of the La^{3+}. Consequently, the modeling of the third shell in the other samples is not relevant in the frame of this study since there is an uncertainty on the real nature of the peaks at this distance (noise or W atoms).

In addition, the FT of the experimental La⊂{NH_2}-SBA-15 and La⊂POM-COOH@{NH_2}-SBA-15(1:1) EXAFS spectra were compared (Figure 6, bottom). This comparison is instructive since the peaks corresponding to the first shells are not superimposable, in terms of mean distance and width. The La-O distances distribution in La⊂POM-COOH@{NH_2}-SBA-15(1:1)

is thus narrow and can be modeled with a single set of 8 O atoms located at 2.658 (± 0.053) Å ($|\sigma^2|$ = 0.0102), close to what was calculated for the model compound. The calculated distances obtained for La-As and La-P are respectively 3.538 (± 0.167) Å and 3.939 (± 0.094) Å, and are also in accordance with the structural data of the molecular model La⊂POM-COOH. This data was modeled by taking into account the same 8 FEFF paths used for La⊂POM-COOH.

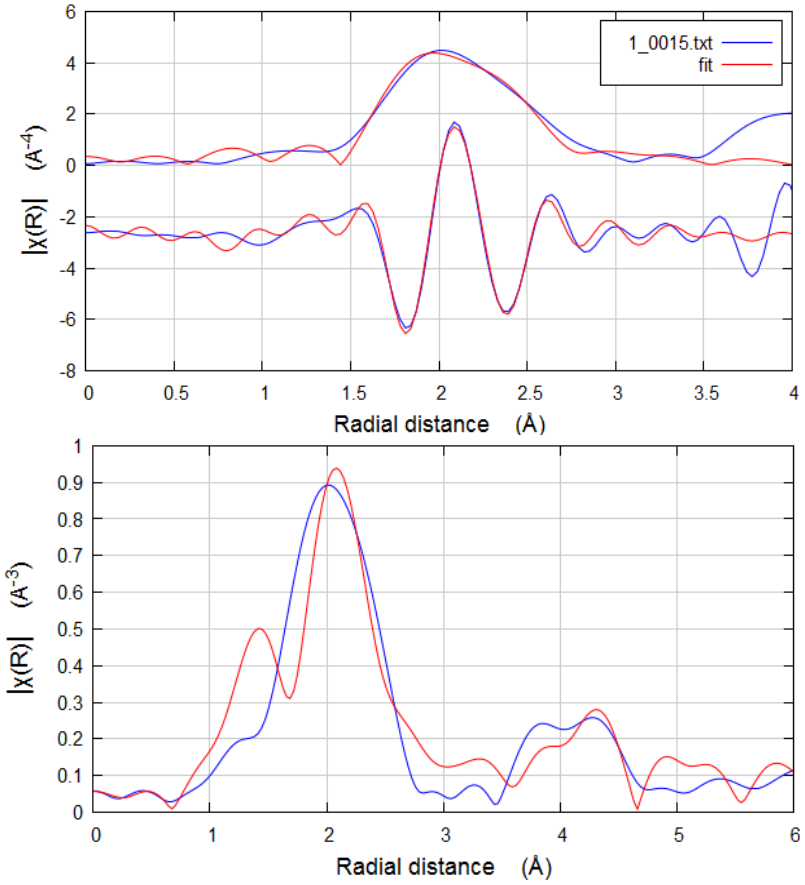

Figure 6. (Top) Calculated (red) and experimental (blue) FT of the first shell of La⊂{NH_2}-SBA-15 EXAFS spectrum (calculation in the range 1.5 - 4 Å). (Bottom) Comparison of the FT of the experimental La⊂{NH_2}-SBA-15 (blue) and La⊂POM-COOH@{NH_2}-SBA-15(1:1) (red) EXAFS spectra.

Finally, the La-O distributions for the different La⊂POM-COOH@{NH_2}-SBA-15(x:1) samples were also compared in Figure 7. These La-O distances (in the range 2 to 2.7 Å) were found dependent on the x ratio. Indeed for x = 0.75 and 1, the top of the peak attributed to the La-O shells was at the R position corresponding to the exact distance observed in La⊂POM-COOH. On the contrary, the peak observed for x = 2 was significantly displaced towards the lower value of R. The position of this peak was very similar to what was observed with La⊂{NH_2}-SBA-15. This is probably due to a poor defined spectrum of this particular sample, which is the most disordered of all. Indeed, average EXAFS signals are obtained if two or more different environments for the target element exist in the materials. This is thus the case in the present study when x is strictly greater than 1. Consequently, as expected, the main band associated to the first shell (in the range 2 to 2.7) is larger in the case of La-POM-COOH@{NH_2}-SBA-15(2:1) compared to the samples where x = 0.75 and 1, reflecting an important disorder associated to the presence of different La sites in the materials. However, the presence of POMs in the vicinity of part of the La atoms is attested by the presence of the peaks corresponding to the second shell in the range 2.7 to 3.5 Å (while lower than the samples where $x \leq 1$), as expected.

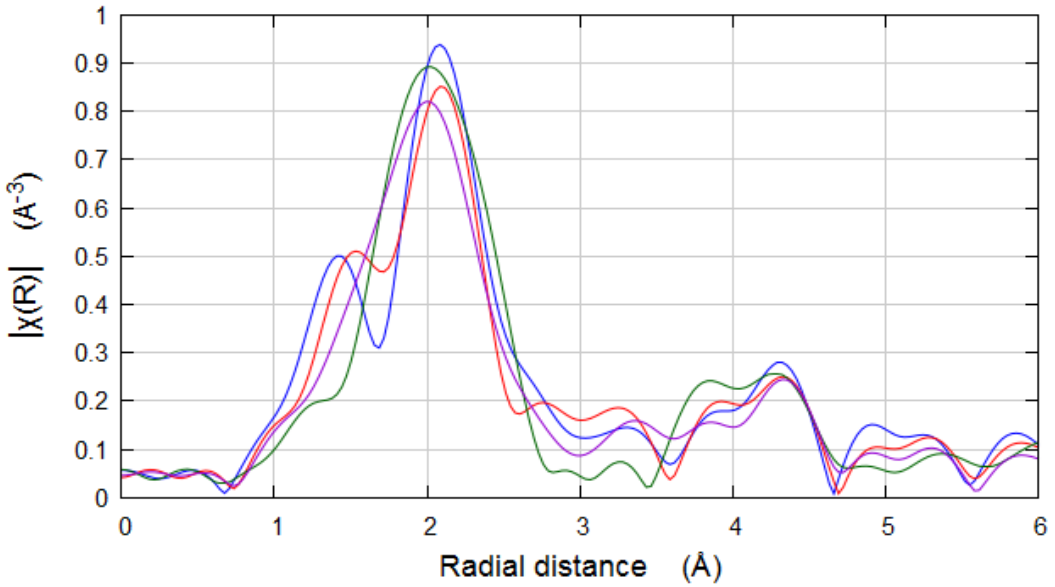

Figure 7. Comparison of the FT of La⊂POM-COOH@{NH_2}-SBA-15(x:1) samples with x = 0.75 (red), 1 (blue), 2 (violet) EXAFS spectra, and of La⊂{NH_2}-SBA-15 (green).

Conclusion

In conclusion, on the basis of the CP-MAS ^{31}P NMR and EXAFS study, it seems certain that for x < 1, the La^{3+} ions introduced in the POM-COOH@{NH_2}-SBA-15(x:1) materials are, for the most part, coordinated by the POMs that are linked to the mesoporous supports. Indeed, even if the W atoms originate from POM-COOH are hardly observable in the vicinity of La^{3+} ions (due to a high signal-over-noise ratio in the experimental conditions used), the second shell of neighbors can be fairly modeled by taking into account the presence of As and P atoms from POM-COOH. Furthermore, the La-O distances and distribution are in accordance with those observed in the molecular model compound La⊂POM-COOH. Finally, for x > 1, the extra La^{3+} ions introduced in the materials have a local environment identical to La^{3+} ions found in La⊂{NH_2}-SBA-15, as expected. It is noteworthy that this environment can be distinguished from that of POMs-coordinated La^{3+} ions by using EXAFS.

Finally, it should be reminded that we have previously shown that the formation of amide bond between the phosphonyle derivatives of POMs and the mesoporous support led to the non aggregation of the POMs onto the support, thus to a regular distribution of the POMs within the channels of {NH_2}-SBA-15. All together, these results thus demonstrate that, due to the selective uptake of La^{3+} by the POMs in these materials, these new hybrid materials allow a particularly fine dispersion of La^{3+} at the surface of SBA-15, that gives hopes for promising catalytic properties for the La^{3+} ions.

Associated Content. Structure of the polymeric compound $\{[AsW_9O_{33}\{P(O)CH_2CH_2CO_2H\}_2\{La(dmf)(H_2O)_2\}]^{2-}\}_x$; Normalized X-Ray absorption spectrum of La⊂POM-COOH; Synthesis and characterization of POM-COOH and La⊂POM-COOH; Normalized Small Angles X-ray diffractograms and Normalized nitrogen adsorption-desorption isotherms of the samples; Additional micrographs (after microtome cuttings) of the preliminary sample of La⊂POM-COOH@{NH_2}-SBA-15. The following files are available free of charge.

Corresponding Author

* Sorbonne Université, CNRS UMR 8232, Institut Parisien de Chimie Moléculaire, Campus Pierre et Marie Curie, 4 Place Jussieu, F-75005 Paris, France. E-mail: richard.villanneau@sorbonne-universite.fr.

Author Contributions

The manuscript was written through contributions of all authors. All authors have given approval to the final version of the manuscript. ‡

ACKNOWLEDGMENT

This work was supported by the Centre National de la Recherche Scientifique (CNRS) and the Université Pierre et Marie Curie – Paris 6 (Sorbonne Université), in particular for funding Dr Faiza Lilia Bentaleb as assistant lecturer. The authors acknowledge support from the Ministère de la Recherche et de l'Enseignement Supérieur for a PhD fellowship to Miss Ourania Makrygenni. The authors want also to acknowledge SOLEIL synchrotron (L'Orme des Merisiers Saint-Aubin, Gif-sur-Yvette, France) for provision of synchrotron radiation facilities and would like to thank Dr Andrea Zitolo for assistance in using beamline SAMBA (proposal 20160268), Pr. Xavier Carrier (from Laboratoire de Réactivité de Surface, CNRS-UMR 7197, Sorbonne Université) for his help with the EXAFS analysis and Mr Matthieu Balas for the Normalized Small Angles X-ray diffractograms and Normalized nitrogen adsorption-desorption isotherms of the samples.

ABBREVIATIONS

CP-MAS NMR: Cross-Polarized Magic Angle Spinning Nuclear Magnetic Resonance; EXAFS: Extended X-Ray Absorption Fine Structure; FT: Fourier Transform; POMs: Polyoxometalates; SBA-15: Santa Barbara Amorphous-15 mesoporous silica; XAS: X-ray Absorption Spectroscopy; X-EDS = X-Ray Energy-Dispersive Spectroscopy.

REFERENCES

[1] (a) B. R. Baker, Advances in the Chemistry of the Coordination Compounds. J. Am. Chem. Soc. 84 (1962) 1515–1516, DOI: 10.1021/ja00867a056. (b) M. T. Pope, Heteropoly and Isopoly Oxometalates, Springer-Verlag, 1983. (c) Ed. J. J. Borrás-Almenar, E. Coronado, A. Müller, M. T. Pope, Polyoxometalate Molecular Science, Springer Netherlands, 2003.

[2] (a) N. Mizuno, K. Kamata, K. Yamaguchi, Green Oxidation Reactions by Polyoxometalate-Based Catalysts: From Molecular to Solid Catalysts. Top. Catal. 53 (2010) 876-893, DOI 10.1007/s11244-010-9520-x. (b) Ed. C.L. Hill Special Issue on Polyoxometalates in Catalysis. J. Mol. Cat. A: Chem. 262 (2007) 1-242. (b) I. V. Kozhevnikov, Catalysts for Fine Chemical Synthesis Vol. 2: Catalysis by Polyoxometalates (2002) Wiley, Eds: S. M Roberts, I. V Kozhevnikov, E. Derouane. (c) N. Mizuno, K. Yamaguchi, K. Kamata, Epoxidation of olefins with hydrogen peroxide catalyzed by polyoxometalates. Coord. Chem. Rev. 249 (2005) 1944-1956, DOI: 10.1016/j.ccr.2004.11.019. (d) R. Neumann, Activation of molecular oxygen, polyoxometalates, and liquid-phase catalytic oxidation. Inorg. Chem. 49 (2010) 3594-3601, DOI: 10.1021/ic9015383. (e) N. Mizuno, K. Kamata, Catalytic Oxidation of hydrocarbons with hydrigen peroxide by Vanadium-based polyoxometalates. Coord. Chem. Rev. 255 (2011) 2358-2370, DOI: 10.1016/j.ccr.2011.01.041. (f) K. Kamata, K. Yonehara, Y. Nakagawa, K. Uehara, N. Mizuno, Efficient stereo- and regioselective hydroxylation of alkane catalysed by a bulky polyoxometalate. Nat. Chem. 2 (2010) 478-483, DOI: 10.1038/NCHEM.648. (g) N. V Maksimchuk, G. M.Maksimov, V. Y. Evtushok, I. D. Ivanchikova, Y. A Chesalov, R. I. Maksimovskaya, O. A. Kholdeeva, A. Solé-Daura, J.M. Poblet, J.J. Carbo, Relevance of Protons in Heterolytic Activation of H_2O_2 over Nb(V). Insights from Model Studies on Nb-substituted Polyoxometalates. ACS Catal. 8 (2018) 9722-9737, DOI: 10.1021/acscatal.8b02761. (h) T. Zhang, L. Mazaud, L.-M. Chamoreau, C. Paris, G. Guillemot, Unveilling the active surface sites in heterogeneous titanium-based silicalite epoxidation catalysts: input of silanol-functionalized polyoxotungstates as soluble analogues. ACS Catal. 8 (2018) 2330-2342, DOI: 10.1021/acscatal.8b00256.

[3] (a) R. Contant, Relations entre les tungstophosphates apparentés à l'anion $PW_{12}O_{40}^{3-}$. Synthèse et propriétés d'un nouveau polyoxotungstophosphate lacunaire $K_{10}P_2W_{20}O_{70}{\cdot}24H_2O$. Can. J. Chem. 65 (1987) 568-573, DOI: 10.1139/v87-100. (b) I. A Weinstock, J. J. Cowan, E.M.G. Barbuzzi, H. Zeng, C. L. Hill, Equilibria between α and β Isomers of Keggin Heteropolytungstates. J. Am. Chem. Soc. 121 (1999) 4608-4617, DOI: 10.1021/ja9955316 (c) A. Tézé, G. Hervé, Relationship between structures and properties of undecatungstosilicate isomers and of some derived compounds. J. Inorg. Nucl. Chem. 39 (1977) 2151-2154, DOI: 10.1016/0022-1902(77)80384-9. (d) R. Contant, R. Thouvenot, Y. Dromzée, A. Proust, P. Gouzerh, Synthesis and Structural Chemistry of Tungstoarsenates(V). J. Clust. Sci. 17 (2006) 317-331, DOI: 0.1007/s10876-006-0054-0. (e) D. K. Lyon, W. K. Miller, T. Novet, P. J. Domaille, E. Evitt, D. C. Johnson, R. G. Finke. Highly oxidation resistant inorganic-porphyrin analog polyoxometalate oxidation catalysts. 1. The synthesis and characterization of aqueous-soluble potassium salts of α_2-$P_2W_{17}O_{61}(M^{n+}{\cdot}OH_2)^{(n-10)-}$ and organic solvent soluble tetra-*n*-butylammonium salts of α_2-$P_2W_{17}O_{61}(M^{n+}{\cdot}Br)^{(n-11)-}$ (M = Mn^{3+}, Fe^{3+}, Co^{2+}, Ni^{2+}, Cu^{2+}). J. Am. Chem. Soc. 113 (1991) 7209-7221, DOI: 10.1021/ja00019a018.

[4] C. Rong, M. T. Pope, Lacunary polyoxometalate anions are pi-acceptor ligands. Characterization of some tungstoruthenate(II,III,IV,V) heteropolyanions and their atom-transfer reactivity. J. Am. Chem. Soc. 114 (1992) 2932-2938, DOI: 10.1021/ja00034a027.

[5] A. Proust, B. Matt, R. Villanneau, G. Guillemot, P. Gouzerh, G. Izzet, Functionalization and post-functionalization: a step towards polyoxometalate-based materials. Chem. Soc. Rev. 41 (2012) 7605-7622, DOI: 10.1039/C2CS35119F.

[6] R. Villanneau, A. Marzouk, Y. Wang, A. Ben Djamaa, G. Laugel, A. Proust, F. Launay, Covalent Grafting of Organic–Inorganic Polyoxometalates Hybrids onto Mesoporous SBA-15: A Key Step for New Anchored Homogeneous Catalysts. Inorg. Chem. 52 (2013) 2958-2965, DOI: 10.1021/ic302374v.

[7] O. Makrygenni, E. Secret, A. Michel, D. Brouri, V. Dupuis, A. Proust, J.-M. Siaugue, R. Villanneau, Heteropolytungstate-decorated core-shell magnetic nanoparticles: A covalent strategy for polyoxometalate-based hybrid nanomaterials. J. Colloid Interface Sci. 514 (2018) 49-58, DOI: 10.10116/j.jcis.2017.12.019.
[8] O. Makrygenni, D. Brouri, A. Proust, F. Launay, R. Villanneau, Immobilization of polyoxometalate hybrid catalysts onto mesoporous silica supports using phenylene diisothiocyanate as a cross-linking agent. Microporous Mesoporous Mater. 278 (2019) 314-321, DOI: 10.10116/micromeso.2018.11.036.
[9] F. Bentaleb, O. Makrygenni, D. Brouri, C. Coelho Diogo, A. Mehdi, A. Proust, F. Launay, R. Villanneau, Efficiency of Polyoxometalate-Based Mesoporous Hybrids as Covalently Anchored Catalysts. Inorg. Chem. 54 (2015) 7607-7616, DOI: 10.1021/acs.inorgchem.5b01216.
[10] R. Villanneau, D. Racimor, E. Messner-Henning, H. Rousselière, S. Picart, R. Thouvenot, A. Proust, Insights into the Coordination Chemistry of Phosphonate Derivatives of Heteropolyoxotungstates. Inorg. Chem. 50 (2011) 1164–1166, DOI: 10.1021/ic102223w.
[11] R. Villanneau, A. Ben Djamâa, L. M. Chamoreau, G. Gontard, A. Proust, Bisorganophosphonyl and -Organoarsenyl Derivatives of Heteropolytungstates as Hard Ligands for Early-Transition-Metal and Lanthanide Cations. Eur. J. Inorg. Chem. 10-11 (2013) 1815–1820, DOI: 10.1002/ejic.201201257.
[12] M. Hatano, K. Ishihara, Lanthanum(III) catalysts for highly efficient and chemoselective transesterification. Chem. Commun. 49 (2013) 1983-1997, DOI: 10.1039/c2cc38204k.
[13] (a) S. Liao, S. Yu, Z. Chen, D. Yu, L. Shi, R. Yang, Q. Shen, Diels-Alder reaction catalyzed by lanthanide chlorides. J. Mol. Catal. 72 (1992) 209-219, DOI: 10.1016/0304-5102(92)80046-J. (b) C. Qi, Y. Xiong, V. Eschenbrenner-Lux, H. Cong, J. A. Porco, Asymmetric syntheses of the flavonoid Diels-Alder natural products Sanggenons C and O. J. Am. Chem. Soc. 138 (2016) 798-801, DOI:10.1021/jacs.5b12778.
[14] A. Dzudza, T. J. Marks, Lanthanide Triflate-Catalyzed Arene Acylation. Relation to Classical Friedel–Crafts Acylation. J. Org. Chem. 73 (2008) 4004-4016, DOI: 10.1021/jo800158k.
[15] D. Li, G. Chen, X. Wang, Incorporation of lanthanum into SBA-15 and its catalytic activity in trichloroethylene combustion. J. Rare Earth 26 (2008) 717-721, DOI: 10.1016/S1002-0721(08)60169-6.
[16] (a) X. L. Sheng, Y. M. Zhou, Y. Z. Duan, Y. W. Zhang, M.W. Xue, Effect of different lanthanum source and preparation method on the lanthanum-doped mesoporous SBA-15 synthesis. J. Porous Mat. 18 (2011) 677–683, DOI: 10.1007/s10934-010-9426-9. (b) X. Sheng, Y. Zhou, Y. Zhang, Y. Duan, Z. Zhang, Y. Yang, Immobilization of 12-Tungstophosphoric acid in alumina-grafted mesoporous LaSBA-15 and its catalytic activity of *o*-xylene styrene. Microporous Mesoporous Mater. 161 (2012) 25-32, DOI: 10.1016/j.micromeso.2012.05.025. (c) J. Liu, Y. Liu, W. Yang, H. Guo, F. Fang, Z. Tang, Immobilization of phosphotungstic acid on amino-functionalized bimetallic Zr–La-SBA-15 and its highly catalytic performance for acetylation. J. Mol. Catal A-Chem. 393 (2014) 1-7, DOI: 10.1016/j.molcata.2014.04.011.
[17] (a) V. Lahootun, C. Besson, R. Villanneau, F. Villain, L.-M. Chamoreau, K. Boubekeur, S. Blanchard, R. Thouvenot, A. Proust, Synthesis and Characterization of the Keggin-Type Ruthenium-Nitrido Derivative $[PW_{11}O_{39}\{RuN\}]^{4-}$ and Evidence of its Electrophilic Reactivity. J. Am. Chem. Soc. 129 (2007) 7127-7135, DOI: 10.1021/ja071137t. (b) R. Villanneau, A. Proust, F. Robert, F. Villain, M. Verdaguer, P. Gouzerh, Polyoxoanion-supported pentamethylcyclopentadienylrhodium complexes: syntheses, crystal structures and EXAFS studies. Polyhedron 22 (2003) 1157-1165, DOI: 10.1016/S0277-5387(03)00040-8. (c) H. Carabineiro, R. Villanneau, X. Carrier, P. Herson, F. Lemos, F. R. Ribeiro, A. Proust, M. Che, Zirconium-substituted isopolytungstates: structural models for zirconia-supported tungsten catalysts. Inorg. Chem. 45 (2006) 1915-1923, DOI: 10.1021/ic051941l.
[18] (a) G. Absilis, R. Van Deun, T. N. Parac-Vogt, Polyoxomolybdate Promoted Hydrolysis of a DNA-Model Phosphoester Studied by NMR and EXAFS Spectroscopy. Inorg. Chem. 50 (2011) 11552–11560, DOI: 10.1021/ic201498u. (b) R. Schiwon, K. Klingan, H. Dau, C. Limberg, Shining light on integrity of a tetracobalt-polyoxometalate water oxidation catalyst by X-ray spectroscopy before and after catalysis.

Chem. Commun. 50 (2014) 100-102, DOI: 10.1039/C3CC46629A. (c) M. S. S. Balula, I. C. M. S. Santos, J. A. F.Gamelas, A. M. V. Cavaleiro, N. Binsted, W. Schlindwein, Structural Studies of Keggin-Type Polyoxotungstates by Extended X-ray Absorption Fine Structure Spectroscopy. Eur. J. Inorg. Chem. 7 (2007) 1027-1038, DOI: 10.1002/ejic.200500681. (d) M. - H. Chiang, M. R. Antonio, C. W. Williams, L. Soderholm, A unique coordination environment for an ion: EXAFS studies and bond valence model approach of the encapsulated cation in the Preyssler anion. Dalton Trans. 2004, 801-806, DOI: 10.1039/B315334G. (e) A. J. Gaunt, I. May, M. Helliwell, S. Richardson, The First Structural and Spectroscopic Characterization of a Neptunyl Polyoxometalate Complex. J. Am. Chem. Soc. 124 (2002) 13350-13351, DOI: 10.1021/ja028005e. (f) M. Nishio, S. Inami, M. Katayama, K. Ozutsumi, Y. Hayashi, Lanthanide Complexes of Macrocyclic Polyoxovanadates by VO_4 Units: Synthesis, Characterization, and Structure Elucidation by X-ray Crystallography and EXAFS Spectroscopy. Inorg. Chem. 51 (2012) 784-793, DOI: 10.1021/ic200638f. (g) B. Monteiro, S. S. Balula, S. Gago, C. Grosso, S. Figueiredo, A. D. Lopes, A. A. Valente, M. Pillinger, J. P. Lourenço, I. S. Gonçalves, Comparison of liquid-phase olefin epoxidation catalysed by dichlorobis-(dimethylformamide)dioxomolybdenum(VI) in homogeneous phase and grafted onto MCM-41. J. Mol. Catal A-Chem. 297 (2009) 110-117, DOI: 10.1016/j.molcata.2008.09.012.

[19] Data for all samples were collected in transmission mode after dilution in cellulose. XAS data analysis was carried out with the Demeter package: Ravel, B.; Newville M. ATHENA, ARTEMIS, HEPHAESTUS: data analysis for X-ray absorption spectroscopy using IFEFFIT. J. Synchrotron Rad. 12 (2005) 537-541, DOI: 10.1107/S0909049505012719.

[20] S.I. Zabinsky, J. J. Rehr, J. J. Ankudinov, R. C. Albers, M. J. Eller, Multiple Scattering calculations of X-ray absorption spectra. Phys. Rev. B 52 (1995) 2995-3009.